Molecular Oxygen Reduction in PEM Fuel Cells: Evidence for the Simultaneous Presence of Two Active Sites in Fe-Based Catalysts

M. Lefèvre and J. P. Dodelet*

INRS-Énergie et Matériaux, C. P. 1020, Varennes, Quebec, Canada, J3X 1S2

P. Bertrand

PCPM, Université Catholique de Louvain, 1348 Louvain-la-Neuve, Belgium

Received: January 29, 2002; In Final Form: April 20, 2002

Three catalysts for the electroreduction of oxygen have been prepared by pyrolyzing between 400 and 1000 °C two iron precursors (Fe acetate or Fe porphyrin) adsorbed on a synthetic carbon made from the pyrolysis of PTCDA (perylene tetracarboxylic dianhydride) in a $H_2/NH_3/Ar$ atmosphere. One Fe loading (0.2 wt %) has been used for the catalyst made from the salt precursor. Two Fe loadings (0.2 and 2.0 wt %) have been used for the catalyst made from the porphyrin precursor. These three catalysts have been analyzed by ToF SIMS and RDE (or GDE) in order to find correlations between ions detected by ToF SIMS and the catalytic activity. These correlations provide information about the number and the structure of the catalytic sites, which are active in these materials. By following the variation of $FeN_xC_y^+$ ions, it is found that (i) two different catalytic sites exist simultaneously in all catalysts made with the Fe salt or the Fe porphyrin; (ii) one site, named FeN_4/C, is at the origin of three families of $FeN_xC_y^+$ ions: $FeN_4C_y^+$, $FeN_3C_y^+$, and $FeN_1C_y^+$. The most representative ion of that site is $FeN_4C_8^+$. The other site, labeled FeN_2/C, is at the origin of the family of $FeN_2C_y^+$ ions. The most representative ion of that site is $FeN_2C_4^+$; (iii) the abundance of FeN_2/C goes through a maximum for catalysts pyrolyzed between 700 and 900 °C. When Fe acetate is the Fe precursor, FeN_2/C may represent up to 80% of the catalytic sites, while this falls to a maximum of about 50% when Fe porphyrin is the precursor; (iv) FeN_2/C is more electrocatalytically active than FeN_4/C; (v) at high porphyrin loading (2.0 wt % Fe), the catalytic sites bound to the carbon support are covered with a porous layer of pyrolyzed Fe porphyrin.

Introduction

Non-noble metal catalysts for the reduction of oxygen in polymer electrolyte membrane (PEM) fuel cells are a subject of current interest. As PEM fuel cells function at about pH = 1,[1] it is, therefore, not possible to use cathode catalysts made of non-noble metal particles, which would rapidly corrode in such acidic conditions. However, it has been known for several years that N_4-metal macrocycles (tetraazaannulenes, porphyrins, and phthalocyanines) and other N_4-metal chelates with metal = Fe or Co, adsorbed on carbon and heat-treated at various temperatures, are catalysts for the reduction of O_2 in acidic medium.[2−29] The best electrocatalytic activities were shown to occur in the pyrolysis temperature range between 500 and 700 °C. In that temperature range, it has been proposed that the catalytic site is N_4-metal bound to the carbon support.[11,30] This site has been named "the low-temperature catalytic site".[31] Another catalytic site, labeled "the high-temperature catalytic site",[31] has also been detected at pyrolysis temperatures ≥ 800 °C.[31−43] The complete structure of this second site is not yet known. However, some information about its formation and its composition has been collected. So far, it is known that:

(i) C, N, and Fe (or Co) are necessary to obtain that catalytic site. C is either carbon black or activated carbon. A carbon precursor may also be used as, for instance, polyacrylonitrile (PAN[33]) or perylene tetracarboxylic dianhydride (PTCDA[31,44,45]). The precursor of N may be NH_3[31,44,45] or CH_3CN,[38,43] or N-containing molecules such as N_4-Me macrocycles. The precursor of Fe (or Co) may be an Fe (or Co) macrocycle but it may also be an Fe (or Co) salt as in refs 33, 43, and 44.

(ii) From XPS experiments on Fe-based catalysts,[44,45] it is known that, to obtain a catalyst, the nitrogen atoms on the carbon support have to be of the pyridinic type (N contributing one π electron to the conjugation of the graphene plane of the carbon support and having two other electrons in an n orbital).

(iii) From Time-of-Flight Secondary Ion Mass Spectrometry (ToF SIMS) on Fe-based catalysts,[31] it is also known that the pyridinic-type nitrogens have to be in a structure of the phenanthroline type (see Figure 1), to be able to coordinate the Fe ion in the catalytic site. When such nitrogen atoms exist on the carbon support, adding Fe ions (even 50 ppm) induces catalytic activity. Increasing the Fe content increases the concentration of the catalytic sites until all nitrogens of the phenanthroline type are coordinated with Fe. This site saturation occurs around 0.5 wt % Fe, when Fe acetate is used as Fe precursor[44] and around 2 wt % Fe, when a porphyrin like Cl-Fe tetramethoxyphenyl porphyrin (Cl-FeTMPP) is used as Fe precursor.[31] Increasing the Fe content further produces Fe metal (and/or carbide) particles that induce graphitization around them.[46] These particles are catalytically inactive.[36]

ToF SIMS experiments have been performed and correlated with Rotating Disk Electrode (RDE) or Gas Diffusion Electrode

* Author to whom correspondence should be addressed. E-mail: dodelet@inrs-ener.uquebec.ca.

10.1021/jp020267f CCC: $22.00
Published on Web 07/27/2002

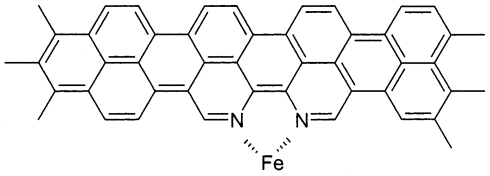

Figure 1. Proposed moiety of the high-temperature catalytic site.

(GDE) experiments in order to obtain more information about the structure of both catalytic sites. These experiments have been performed on three types of catalysts using pyrolyzed PTCDA at 900 °C in $H_2/NH_3/Ar$ atmosphere as synthetic carbon support. The first type of catalysts uses Fe acetate as Fe precursor with an Fe content of 0.2 wt %. The second and third types of catalysts use both Cl-FeTMPP as Fe precursor with an Fe content of either 0.2 or 2.0 wt %. The two Fe precursors, which are adsorbed on the pre-pyrolyzed PTCDA, are pyrolyzed a second time in a H_2/Ar atmosphere at various temperatures ranging from 400 to 1000 °C in order to obtain a large range of catalytic activities. This procedure is labeled Procedure II in order to reflect the two-pyrolysis steps used to produce the catalysts. It will be shown that it is erroneous to make a distinction between low- and high-temperature catalytic sites since both sites exist simultaneously at all pyrolysis temperatures between 400 and 1000 °C for both Fe precursors used. However, these sites do not have the same catalytic activity, the former high-temperature site being the most active one.

Experimental Section

Preparation of the Catalysts. The purification of perylene tetracarboxylic dianhydride (PTCDA) and its pyrolysis to obtain a synthetic carbon support were already described.[31] Three types of catalyst samples have been prepared. The preparation procedures are all derived from Procedure II, which is defined in the Introduction. The samples were labeled to reflect the origin of their Fe precursor and their preparation conditions.

Samples of Type II Fe(0.2)Ac. An amount of Fe^{II} acetate (Aldrich) required to obtain a nominal Fe content of 2000 ppm (0.2 wt %) in the catalyst was mixed with a magnetic stir bar for 1 h with a suspension of pre-pyrolyzed PTCDA in 100 mL of $d.H_2O$. The mixture was dried at 75 °C for one night. The resulting material was placed in a fused silica boat and introduced in the fused silica tubular reactor. The pyrolysis temperatures examined were 400, 500, 600, 700, 800, 900, and 1000 °C. The pyrolysis atmosphere was Ar/H_2 in a 1:1 volumetric ratio. The actual Fe content was measured by Neutron Activation Analysis (NAA) for the catalyst prepared at 900 °C and found to be 2011 ppm ± 5%.

Samples of Type II Fe (0.2)P. An amount of $Cl-Fe^{III}$ tetramethoxyphenylporphyrin (Cl-FeTMPP from Aldrich) required to obtain a nominal Fe content of 0.2 wt % in the catalyst was mixed for 1 h with a suspension of pre-pyrolyzed PTCDA in 100 mL acetone. The acetone was evaporated and the product was dried at 75 °C for one night. The pyrolysis procedure and temperatures are the same as for samples of type II Fe(0.2)Ac.

Samples of Type II Fe(2.0)P. These samples were prepared exactly as samples of type II Fe(0.2)P, except that the nominal Fe content was 20 000 ppm (2.0 wt %) instead of 2000 ppm. One sample of the same type was also prepared with Co^{II} tetramethoxy phenyl porphyrin (CoTMPP from Aldrich) instead of Fe. The pyrolysis temperature of that sample was 900 °C. It was labeled II Co(2.0)P.

Electrochemical Measurements. The catalysts were evaluated electrochemically in half-cells. Measurements were obtained by the rotating disk electrode technique (RDE). The procedure to prepare the catalytic film was the following: 16 mg of finely ground catalyst, 0.400 mL of $d.H_2O$, and 0.400 mL of a 5 wt % Nafion in alcohol−water solution (Aldrich) were ultrasonically blended for 10 min. Then 10 μL of this suspension was pipetted onto the 5 mm diameter vitreous carbon disk of the electrode. The suspension was dried in air at 75 °C. RDE measurements were performed at room temperature in a three-electrode, one-compartment cell containing H_2SO_4 (pH = 1) as the electrolyte. It was saturated with O_2 prior to the start of each experiment. Cyclic voltammograms were recorded at a scan rate of 10 mV s^{-1} between − 0.3 and 0.7 V vs SCE. Typical RDE voltammetric results are presented in Figure 1 of ref 31. The disk electrode is not rotated during the first scan, giving only one peak for O_2 reduction in O_2-saturated H_2SO_4. The second scan is recorded at 1500 rpm. The magnitude of the reduction currents improves due to the increase of the available O_2 supplied by the forced convection arising from electrode rotation. It is possible to estimate the relative catalytic activity of several catalysts by measuring the potential, V_{pr}, at which the maximum reduction occurs at 0 rpm. V_{pr} values closer to the theoretical reversible potential of 0.985 V vs SCE for the Oxygen Reaction Reduction (ORR) indicate superior catalytic activity.

The measurements in fuel cells were obtained in a fuel cell test station. The procedure to prepare the gas diffusion electrodes (GDE) and assemble the single cells were already described.[31] All fuel cell measurements were performed at 80 °C. The O_2 and H_2 gas back pressures were 60 and 30 psi(gauge) (207 and 414 kPa), respectively. The O_2 and H_2 gas flow rates were 360 and 230 cm^3/min, respectively. The two gases were humidified prior to admission into the fuel cell by passing them through stainless steel containers filled with $d.H_2O$ kept at 105 °C. Before performing any measurements, the fuel cell was left under open circuit conditions for 30 min. Next, a potential of 0.7 V vs RHE was applied during 2.5 h. Then a polarization curve was recorded by varying the applied potential from 0.9 to 0V vs RHE.

Surface Analysis. The surface of the catalyst was analyzed by ToF SIMS (Charles-Evans and Associates) using Ga^+ 15 keV primary ions with a resolution of 10000 for Si on a Si wafer. For the samples, a mass resolution ($m/\Delta m$) of about 4000 at the Si mass (m) is obtained. This mass resolution allowed us to determine without ambiguity the atomic composition of molecular ions containing Fe, N, and C atoms. For the analysis, the catalysts were pressed either into an In sheet or deposited on an Ag foil precoated with a conducting glue. Four regions were analyzed for each sample in positive and negative ions and a mean value was obtained. A 7 keV post acceleration was used with a 0−10000 mass range analysis. The delivered dose was below 10^{12} ions/cm^2, remaining therefore in the static SIMS range.

In this work, the focus was mainly on ions of the $FeN_xC_y^+$ type. Therefore, the recorded ToF SIMS spectra were analyzed to identify these ions. Due to possible slight experimental setting variations between samples (for instance, slight changes in the incident ion beam current, changes of the detection position on the detector, changes in the surface roughness of the catalyst film, etc.), it is very difficult to compare the absolute intensity of any ion (including any $FeN_xC_y^+$ ion) of one catalyst with that of another catalyst made in different conditions (for instance, different pyrolysis temperature, different Fe precursor loading, etc.). This is illustrated in Figure 2 by summing up the absolute intensity of all positive ions (ΣI^+) and recording (ΣI^+) as a

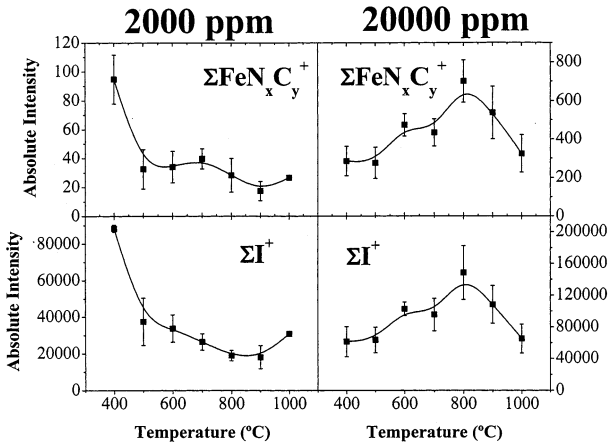

Figure 2. Change with the pyrolysis temperature, in the absolute ToF SIMS intensities of $\Sigma FeN_xC_y^+$ and ΣI^+ for the catalysts made with two Cl-FeTMPP loadings.

function of the pyrolysis temperature for two Cl-FeTMPP loadings. It is clear from Figure 2 that the two curves are different even if the only difference between the two sets of catalysts is only the Cl-FeTMPP loading. The same difference is again detected when one focuses exclusively on $FeN_xC_y^+$ ions and compares the absolute intensity of $\Sigma FeN_xC_y^+$ vs the pyrolysis temperature for the same two sets of catalysts. These curves are also given in Figure 2.

If it is not possible to compare the absolute intensity of $FeN_xC_y^+$ ions for several catalysts, it is however possible to compare their relative intensity, RI, which is obtained according to eq 1:

$$RI_{FeN_xC_y^+} = FeN_xC_y^+/\Sigma FeN_xC_y^+ \quad (1)$$

where $FeN_xC_y^+$ is the absolute intensity of one particular ion in a particular catalyst and $\Sigma FeN_xC_y^+$ represents the sum of the intensities of all $FeN_xC_y^+$ ions, which are detected in the spectrum of the same catalyst. For this normalization, we included in $\Sigma FeN_xC_y^+$ all ions containing up to four nitrogen atoms and up to twelve carbon atoms. Heavier $FeN_xC_y^+$ ions were not considered because it becomes difficult to assign them without ambiguity in the ToF SIMS spectra.

Results and Discussion

The goal of this work is to determine if there is a correlation between the catalytic activity for O_2 reduction in acidic medium (pH = 1), as measured by RDE cyclic voltammetry (or GDE polarization curves), and the relative intensity of one or several $FeN_xC_y^+$ ions detected by ToF SIMS at the surface of the catalysts. $FeN_xC_y^+$ ions have been chosen because it was found (see point (i) in the Introduction) that an O_2 reduction catalyst is obtained when precursors of the three elements are present at the same time in the reactor during its fabrication. The use of PTCDA as carbon precursor in this work is important since it was shown[31] that synthetic carbons obtained by the pyrolysis of PTCDA give a ToF SIMS spectrum with a reduced background as compared with that of a commercial carbon black like Vulcan. The reduced background of PTCDA allows a better detection of some of the $FeN_xC_y^+$ ions that would otherwise be lost in the background spectrum of commercial supports. Two Fe precursors (Fe acetate and Cl-FeTMPP) were chosen to compare RDE and ToF SIMS results. The Fe loading for Fe acetate was set at 0.2 wt % because graphitized metallic (and/or carbidic) iron particles were detected for Fe loadings > 0.5 wt % (see point (iii) in the Introduction). By doing this, ToF SIMS spectra will not be influenced by the presence of noncatalytic species containing Fe. For Cl-FeTMPP, which has more affinity for pyrolyzed PTCDA and therefore spreads better onto that carbon support than Fe acetate, the Fe content should not be >2 wt %. However, to compare both Cl-FeTMPP and Fe acetate as Fe precursors, it was decided, for the porphyrin-based catalyst, to work at two loadings: 0.2 wt % Fe, which is the same loading as for the Fe acetate samples, and 2.0 wt % Fe, which is at the limit of the Fe content above which graphitized metal Fe (and/or carbide) particles start to appear, and is also a loading frequently used in the literature on commercial carbon supports. Changes in ToF SIMS spectra and in the catalytic activity of these catalysts will now be compared as a function of their pyrolysis temperature.

TABLE 1: Relative Abundance in % of $FeN_xC_y^+$ Ions as a Function of the Pyrolysis Temperature for Type II Fe(0.2)Ac Catalysts

ions	400 °C	500 °C	600 °C	700 °C	800 °C	900 °C	1000 °C
$FeNC^+$	28.27	23.82	17.08	0.76	5.76	1.77	2.50
$FeNC_2^+$	0.78	0.00	1.61	2.63	0.00	0.40	2.50
$FeNC_3^+$	0.78	1.41	2.06	1.82	0.63	1.33	7.50
FeN_2C^+	14.94	7.78	4.80	2.38	1.56	2.56	3.75
$FeN_2C_2^+$	1.78	4.70	1.44	0.53	0.63	0.83	0.00
$FeN_2C_3^+$	0.40	1.26	0.53	1.85	0.00	0.93	12.50
$FeN_2C_4^+$	23.92	26.93	46.95	64.89	78.38	76.38	49.86
$FeN_2C_5^+$	1.10	0.00	0.35	2.08	0.00	0.93	0.00
$FeN_2C_6^+$	1.47	0.00	0.64	0.53	1.32	0.40	0.00
FeN_3C^+	1.75	4.97	5.68	1.32	0.00	0.00	2.78
$FeN_3C_2^+$	0.00	1.36	0.00	0.00	1.32	0.42	0.00
$FeN_3C_3^+$	1.78	2.98	1.91	1.82	0.00	0.81	2.78
$FeN_3C_4^+$	0.00	1.10	0.00	1.06	0.00	0.00	0.00
$FeN_3C_5^+$	2.33	0.37	0.29	0.53	1.56	0.85	0.00
$FeN_3C_6^+$	2.64	0.47	0.35	0.76	1.56	0.00	2.78
$FeN_3C_7^+$	0.00	0.00	0.00	0.00	0.00	0.42	0.00
$FeN_3C_8^+$	0.81	3.98	3.36	2.89	0.00	1.67	1.25
$FeN_3C_9^+$	7.33	3.29	1.16	0.76	0.63	3.06	4.03
FeN_4C^+	3.01	0.68	1.12	1.32	0.00	0.42	0.00
$FeN_4C_2^+$	0.34	1.31	1.67	2.38	0.00	0.93	0.00
$FeN_4C_3^+$	0.34	1.89	0.00	0.76	1.56	0.42	0.00
$FeN_4C_4^+$	0.72	0.52	1.08	0.00	0.00	0.42	2.50
$FeN_4C_5^+$	0.40	0.37	2.18	1.32	1.56	0.00	0.00
$FeN_4C_6^+$	0.00	0.00	0.00	0.53	0.00	0.40	1.25
$FeN_4C_7^+$	0.00	0.00	0.00	0.00	0.00	0.00	0.00
$FeN_4C_8^+$	5.08	8.05	5.45	4.17	1.88	4.64	4.03
$FeN_4C_9^+$	0.00	1.72	0.29	1.60	0.00	0.00	0.00
$FeN_4C_{10}^+$	0.00	0.68	0.00	0.00	0.00	0.00	0.00
$FeN_4C_{11}^+$	0.00	0.00	0.00	1.32	0.00	0.00	0.00
$FeN_4C_{12}^+$	0.00	0.37	0.00	0.00	1.67	0.00	0.00

I. ToF SIMS Results. *Catalysts Obtained from Fe^{II} Acetate; Samples of the Type IIFe(0.2)Ac.* Table 1 presents the relative intensities (abundance, in %) of $FeN_xC_y^+$ ions as a function of the pyrolysis temperature for type IIFe(0.2)Ac catalysts. As shown by the dark points in Figure 3, all the ions listed in Table 1 represent, over all pyrolysis temperatures, about $0.17 \pm 0.06\%$ of all positive ions detected by ToF SIMS. This value is obtained by dividing $\Sigma FeN_xC_y^+$ by ΣI^+ for catalysts made with Fe acetate (curves of $\Sigma FeN_xC_y^+$ and ΣI^+ vs pyrolysis temperature were given in Figure 2 for catalysts made with Cl-FeTMPP). All the ions in Table 1 may be grouped in four $FeN_xC_y^+$ families characterized by 1, 2, 3, and 4 nitrogen atoms, respectively, differing only by the number of carbons. Here, we assume that the ions belonging to the same family arise from the same catalytic structure. This assumption allows us to sum up the relative intensities of all the ions in each family and plot the result against the pyrolysis temperature in Figure 4. Two different behaviors are seen in Figure 4: on one hand, $\Sigma FeN_2C_y^+$

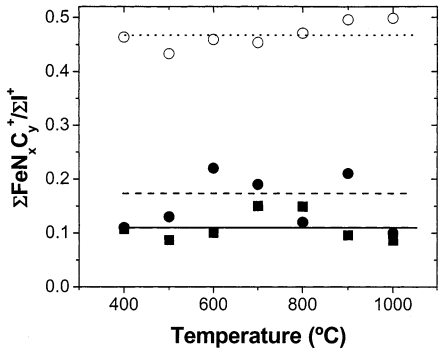

Figure 3. Percentage of the ions of the $FeN_xC_y^+$ type among all positive ions detected by ToF SIMS for: (●) type II Fe(0.2) Ac catalysts; (■) type II Fe(0.2) P catalysts; (○) type II Fe(2.0) P catalysts.

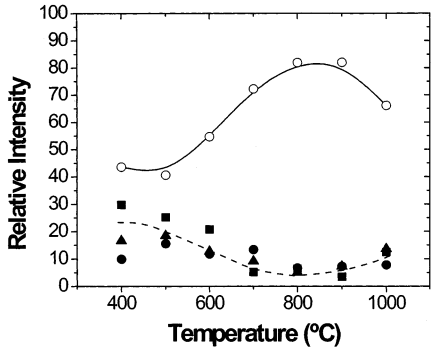

Figure 4. Relative intensity of $\Sigma FeN_2C_y^+$ (○), $\Sigma FeN_1C_y^+$ (■), $\Sigma FeN_3C_y^+$ (▲), $\Sigma FeN_4C_y^+$ (●) as a function of the pyrolysis temperature for type II Fe(0.2) Ac catalysts.

ions increase in intensity with the pyrolysis temperature, go through a maximum at 800−900 °C, then decrease at 1000 °C. On the other hand, the relative intensity of the other three families ($\Sigma FeN_1C_y^+$, $\Sigma FeN_3C_y^+$, and $\Sigma FeN_4C_y^+$ ions) behaves similarly, but with a maximum abundance at 400 °C. From this behavior, one may conclude that the ions belonging to the N_1, N_3, and N_4 families have the same origin: a catalytic site of the FeN_4 type, bound to the carbon support (i.e. the previously labeled low-temperature catalytic site described in the Introduction). On the other hand, the origin of the ions of the N_2 family is a catalytic site of the type FeN_2, bound to the carbon support (i.e., the high-temperature catalytic site, the partial structure of which being depicted in Figure 1).

The distribution between these two sites changes with the temperature. This is illustrated in Figure 5A, in which the stars represent $\Sigma FeN_1C_y^+ + \Sigma FeN_3C_y^+ + \Sigma FeN_4C_y^+$ ions. The two types of catalytic sites coexist at all pyrolysis temperatures and for simplicity we label them FeN_4/C and FeN_2/C. From Figure 5, one sees that FeN_2/C reaches up to 80% of abundance at 800−900 °C. Examining Table 1, it is clear that the FeN_2/C group is composed mainly of $FeN_2C_4^+$ ions, as has been already observed.[31] At the lower pyrolysis temperatures, it is FeN_4/C, which is the most important site. One of the highest abundance ion of that site is $FeN_4C_8^+$ with a mean occurrence of about 5% from 400 to 1000 °C. As the pyrolysis temperature rises, FeN_2/C appears at the expense of the other site.

Catalysts Obtained from Cl-Fe^{III} TMPP; Samples of the Type IIFe(0.2)P. These catalysts have the same Fe content as those of the IIFe(0.2)Ac type, the only difference being the nature of their precursor. Table 2 presents the relative abundance of the $FeN_xC_y^+$ ions as a function of the pyrolysis temperature for the IIFe(0.2)P catalysts. As is shown by the dark squares in Figure 3, all ions listed in Table 2 represent about 0.11 ± 0.04% of all

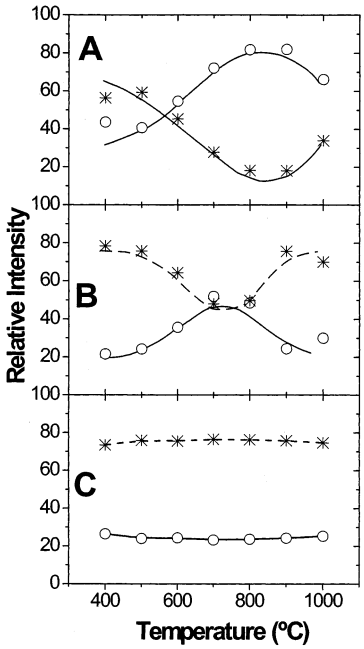

Figure 5. Relative intensity of $\Sigma FeN_2C_y^+$ (○) and (∗): $\Sigma FeN_1C_y^+ + \Sigma FeN_3C_y^+ + \Sigma FeN_4C_y^+$; as a function of the pyrolysis for temperature for three catalysts: (A) II Fe(0.2) Ac; (B) II Fe(0.2) P; (C) II Fe(2.0) P.

TABLE 2: Relative Abundance in % of $FeN_xC_y^+$ Ions as a Function of the Pyrolysis Temperature for the Type II Fe(0.2)P Catalysts

ions	400 °C	500 °C	600 °C	700 °C	800 °C	900 °C	1000 °C
$FeNC^+$	18.39	15.75	14.01	5.56	7.63	15.39	21.67
$FeNC_2^+$	7.05	0.66	6.44	1.69	1.16	4.67	1.67
$FeNC_3^+$	4.99	6.51	2.68	3.38	7.55	5.33	6.67
FeN_2C^+	5.74	5.41	9.10	4.77	6.46	7.36	11.67
$FeN_2C_2^+$	2.23	1.11	0.00	0.71	3.06	1.67	5.00
$FeN_2C_3^+$	1.59	1.57	1.62	0.00	0.00	0.00	1.67
$FeN_2C_4^+$	10.11	11.04	20.23	43.09	34.68	8.00	6.67
$FeN_2C_5^+$	0.98	2.21	2.52	0.98	3.06	1.33	1.67
$FeN_2C_6^+$	0.94	2.87	2.19	2.45	1.26	6.00	3.33
FeN_3C^+	4.55	2.78	3.93	2.45	3.18	3.03	5.00
$FeN_3C_2^+$	1.10	1.70	0.68	0.00	1.19	0.00	0.00
$FeN_3C_3^+$	0.82	1.11	2.19	0.71	0.00	1.33	1.67
$FeN_3C_4^+$	3.62	4.34	2.11	4.67	4.47	4.33	5.00
$FeN_3C_5^+$	5.55	8.64	6.68	6.22	2.45	1.33	8.33
$FeN_3C_6^+$	1.47	0.45	0.94	0.71	0.68	0.00	0.00
$FeN_3C_7^+$	1.85	1.25	0.00	3.16	0.00	0.00	0.00
$FeN_3C_8^+$	3.08	1.25	1.51	1.47	1.77	1.67	1.67
$FeN_3C_9^+$	3.88	4.34	2.31	3.43	3.82	3.03	0.00
FeN_4C^+	2.86	1.11	0.68	2.13	0.68	7.39	0.00
$FeN_4C_2^+$	1.33	1.42	0.47	0.71	3.18	3.33	1.67
$FeN_4C_3^+$	3.14	6.04	2.21	2.22	1.26	4.33	3.33
$FeN_4C_4^+$	0.87	1.77	0.94	0.76	0.00	3.03	1.67
$FeN_4C_5^+$	0.76	1.42	1.99	0.00	0.00	3.03	1.67
$FeN_4C_6^+$	1.37	0.66	1.04	0.00	0.00	0.00	0.00
$FeN_4C_7^+$	1.18	0.00	0.69	0.00	1.26	0.00	0.00
$FeN_4C_8^+$	7.38	11.93	7.61	8.05	10.04	12.73	6.67
$FeN_4C_9^+$	1.89	0.00	3.70	0.00	1.16	1.67	1.67
$FeN_4C_{10}^+$	0.59	0.00	0.00	0.71	0.00	0.00	0.00
$FeN_4C_{11}^+$	0.25	0.00	0.47	0.00	0.00	0.00	0.00
$FeN_4C_{12}^+$	0.47	2.67	1.04	0.00	0.00	0.00	1.67

positive ions detected by ToF SIMS over all pyrolysis temperatures. All ions are again grouped in four families characterized by 1, 2, 3, and 4 nitrogen atoms. Using the same assumption as before (i.e., the ions belonging to the same family arise from the same catalytic site) allows us again to sum up the relative intensities of all the ions in each family and plot the result against the pyrolysis temperature which gives Figure 6. The

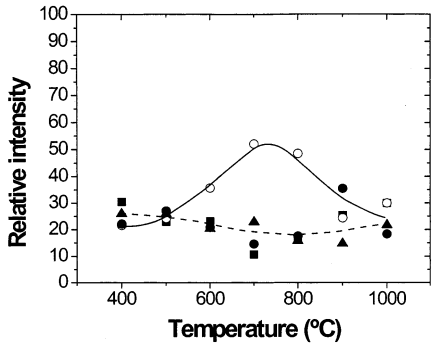

Figure 6. Relative intensity of $\Sigma FeN_2C_y^+$ (○), $\Sigma FeN_1C_y^+$ (*ν*), $\Sigma FeN_3C_y^+$ (▲), $\Sigma FeN_4C_y^+$ (●) as a function of the pyrolysis temperature for type II Fe(0.2) P catalysts.

trend in Figure 6 is similar to that seen in Figure 4 with the N_1, N_3, and N_4 ion families showing one trend and the N_2 family showing another different behavior. The former analysis on the acetate-based catalyst concluding that the ions belonging to the N_1, N_3, and N_4 families have the same origin, (the FeN_4/C catalytic site), and those belonging to the N_2 family are derived from FeN_2/C also holds for the porphyrin-based catalysts made with the porphyrin at 0.2 wt % Fe. Figure 5B is obtained by adding the individual contributions of $\Sigma FeN_1C_y^+ + \Sigma FeN_3C_y^+ + \Sigma FeN_4C_y^+$ ions as it was done for Figure 5A. The most significant difference between the two figures is that the maximum abundance of FeN_2/C is now reduced to 50% and arises in the 700−800 °C range of pyrolysis temperatures. From Table 2, it is seen that $FeN_2C_4^+$, the most representative ion of the FeN_2/C site reaches 43% at 700 °C, while $FeN_4C_8^+$, the most representative ion of the FeN_4/C site reaches a mean value of about 9% over the entire range of pyrolysis temperatures.

Catalysts Obtained from Cl-Fe^{III} TMPP; Samples of the Type IIFe(2.0)P. These catalysts have an Fe content 10 times larger than that of the IIFe(0.2)P type. Table 3 presents the relative abundance for the $FeN_xC_y^+$ ions as a function of the pyrolysis temperature of IIFe(2.0)P catalysts. As is shown by the open points in Figure 3, all ions in Table 3 represent about 0.47 ± 0.03% of all positive ions detected by ToF SIMS over all pyrolysis temperatures (an increase by a factor of 4 compared with IIFe(0.2)P). All ions are again grouped in four families characterized by the number of nitrogen atoms. Using the same assumption as before (i.e., that the ions belonging to the same family arise from the same catalytic site) allow us to sum the relative abundance of all the ions in each family and the results are plotted against the pyrolysis temperature in Figure 7. There is no similarity anymore between Figure 7 and Figures 4 or 6. However, we will continue to assume that the previous conclusion still holds here and that ions belonging to the N_1, N_3, and N_4 families have the same origin: the catalytic FeN_4/C site, and those belonging to the N_2 family belong to FeN_2/C. It allows us to obtain Figure 5C. The open points in Figure 5C represent the contribution of the N_2 family alone (about 25% of all the $FeN_xC_y^+$ ions), while the stars represent the combined contribution of the N_1, N_3, and N_4 families (about 75% of all the $FeN_xC_y^+$ ions). From Table 3, one sees that $FeN_2C_4^+$, which was found as the main ion of the FeN_2/C catalytic site for the other two 0.2 wt % catalysts discussed earlier, is again the main ion, but now has a constant abundance of about 10% over the entire temperature range, while the ion $FeN_4C_8^+$, found earlier as the main ion of the FeN_4/C catalytic site has a constant abundance of about 5% over the entire temperature range.

II. Comparison between Tof SIMS and Electrochemical Results. *Catalysts Obtained from Fe^{II} Acetate; Samples of the Type IIFe(0.2)Ac.* Figure 8 shows the comparison between ToF SIMS relative intensities and RDE oxygen reduction values for type IIFe(0.2)Ac catalysts. The catalytic activity in Figure 8A is evaluated by the value of V_{pr}, the peak reduction potential at 0 rpm in an O_2-saturated H_2SO_4 solution at pH = 1. The curve and open circles in Figure 8B represent the changes in the relative abundance of the FeN_2/C family of ions with pyrolysis temperature and is the same data as was shown in Figure 5. The dark squares in Figure 8B represent the variation of $FeN_2C_4^+$, the main ion characterizing FeN_2/C with the pyrolysis temperature. These results are similar to those already reported in ref 31. Figure 8 demonstrates the good correlation found between the catalytic activity of type IIFe(0.2)Ac catalysts and the relative abundance of ions originating from the FeN_2/C catalytic site. If the FeN_4/C site is active—and it is expected to be so since non-pyrolyzed N_4−Fe macrocycles show activity for the reduction of oxygen[47,48] and a N_4−Fe porphyrin is also

TABLE 3: Relative Abundance in % of $FeN_xC_y^+$ Ions as a Function of the Pyrolysis Temperature for the Type II Fe(2.0)P Catalysts

ions	400 °C	500 °C	600 °C	700 °C	800 °C	900 °C	1000 °C
$FeNC^+$	8.74	9.56	8.02	4.94	3.69	3.55	2.46
$FeNC_2^+$	3.93	3.49	3.01	2.82	2.42	2.58	2.01
$FeNC_3^+$	10.11	13.94	8.75	13.11	12.51	11.42	9.82
FeN_2C^+	5.40	2.91	4.62	2.89	1.37	1.54	1.49
$FeN_2C_2^+$	1.32	1.83	1.32	0.88	0.59	0.79	0.57
$FeN_2C_3^+$	2.35	1.45	1.12	1.54	1.69	1.31	3.70
$FeN_2C_4^+$	12.12	9.22	9.19	10.02	11.12	11.13	9.63
$FeN_2C_5^+$	1.69	2.51	3.60	3.72	4.05	4.16	3.80
$FeN_2C_6^+$	3.66	6.14	4.53	4.27	4.91	5.31	6.12
FeN_3C^+	2.03	1.45	1.89	1.27	1.95	2.33	2.67
$FeN_3C_2^+$	0.49	1.56	0.89	0.79	0.53	0.49	0.28
$FeN_3C_3^+$	4.91	5.77	13.38	13.82	15.26	15.32	13.32
$FeN_3C_4^+$	3.01	4.48	2.14	2.46	2.31	2.63	2.08
$FeN_3C_5^+$	5.51	5.18	4.54	4.95	5.55	5.43	6.29
$FeN_3C_6^+$	2.53	1.35	1.17	1.31	1.02	1.54	1.45
$FeN_3C_7^+$	0.95	0.79	0.42	1.00	0.34	0.32	0.64
$FeN_3C_8^+$	1.27	1.26	1.39	1.08	0.97	1.79	2.65
$FeN_3C_9^+$	6.97	5.74	6.78	8.14	9.11	8.06	11.03
FeN_4C^+	2.77	1.39	2.04	0.59	1.00	0.57	1.04
$FeN_4C_2^+$	1.40	0.09	1.42	0.59	0.65	0.60	0.12
$FeN_4C_3^+$	3.01	3.08	3.57	2.24	1.68	1.91	2.25
$FeN_4C_4^+$	2.27	0.72	0.82	0.41	0.55	1.25	0.60
$FeN_4C_5^+$	1.50	1.74	1.75	0.77	1.09	1.07	1.04
$FeN_4C_6^+$	0.15	0.27	0.34	0.79	0.39	0.37	0.45
$FeN_4C_7^+$	0.40	0.53	0.21	0.36	0.26	0.28	0.40
$FeN_4C_8^+$	4.30	6.05	6.31	5.43	4.34	4.05	3.56
$FeN_4C_9^+$	4.23	3.94	3.84	5.83	6.41	6.05	6.95
$FeN_4C_{10}^+$	1.73	2.17	1.97	2.62	2.40	2.83	2.33
$FeN_4C_{11}^+$	0.49	0.98	0.40	0.45	0.82	0.82	0.60
$FeN_4C_{12}^+$	0.76	0.41	0.59	0.90	1.01	0.52	0.64

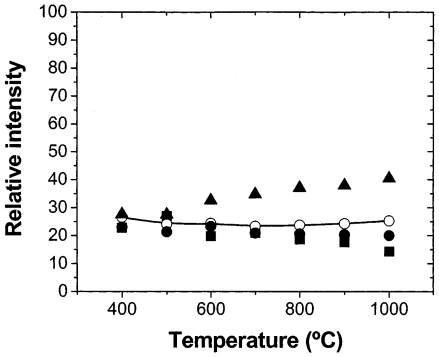

Figure 7. Relative intensity of $\Sigma FeN_2C_y^+$ (○), $\Sigma FeN_1C_y^+$ (■), $\Sigma FeN_3C_y^+$ (▲), $\Sigma FeN_4C_y^+$ (●) as a function of the pyrolysis temperature for type II Fe(2.0) P catalysts.

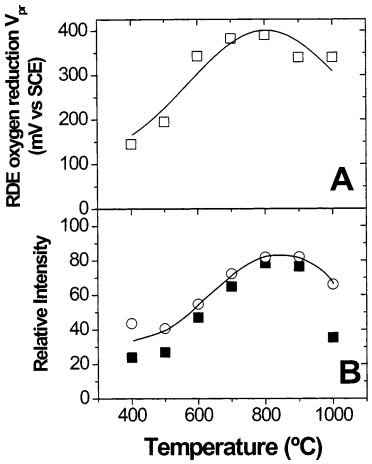

Figure 8. Type II Fe(0.2) Ac catalysts: Comparison between the catalytic activity (as RDE V_{pr}) and the ToF SIMS relative intensity ((■) $FeN_2C_4^+$ only; (○) $\Sigma FeN_2C_y^+$) as a function of the pyrolysis temperature.

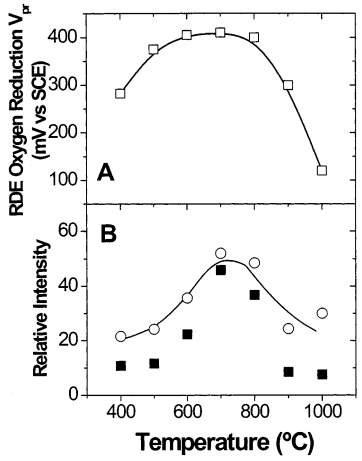

Figure 9. Type II Fe (0.2) P catalysts: Comparison between the catalytic activity (as RDE V_{pr}) and the ToF SIMS relative intensity ((■) $FeN_2C_4^+$ only; (○) $\Sigma FeN_2C_y^+$) as a function of the pyrolysis temperature.

the active site in cytochrome P450, a biological catalyst for O_2 reduction[49]—its contribution to the total activity of the catalysts studied in this work seems, however, minor.

Catalysts Obtained from Cl-Fe^{III} TMPP; Samples of the Type IIFe(0.2)P. Figure 9 shows the RDE-ToF SIMS comparison for type IIFe(0.2)P catalysts. The curve and open circles in Figure 9B are the same data as was shown in Figure 5B, while the dark squares illustrate the variation with the pyrolysis temperature of $FeN_2C_4^+$, which is the main ion characterizing the FeN_2/C site. Again, a similar behavior is found for the two curves in Figures 9A and B. The correlation, however, is not as obvious as was the case in Figure 8 for the IIFe(0.2)Ac catalyst. This disparity is related to the way the catalytic activity is evaluated (a measure of V_{pr} at 0 rpm as described above). A better comparison is given in Figure 10, in which the catalytic activity of the type IIFe(0.2)P catalysts is now expressed in terms of current density measured at a given potential in the activation region, i.e., 0.7 V vs RHE of a polarization curve of the catalyst in a GDE. The entire polarization curves for these same catalysts are presented in Figure 11. At 0.7 V vs RHE, it is expected that the measured current densities are still dominated by the catalytic activity. Going back to Figure 10, given the correlation between ion family abundance and ORR performance, it may again be concluded that the FeN_2/C site dominates the catalytic

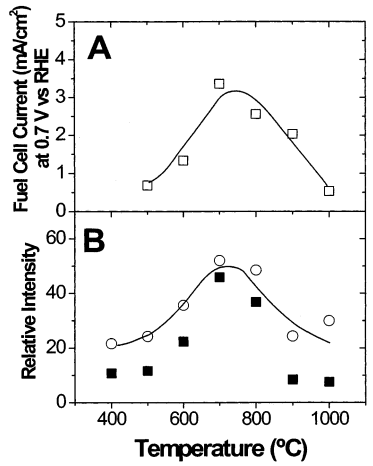

Figure 10. Type II Fe(0.2) P catalysts: Comparison between the catalytic activity (as fuel cell current) and the ToF SIMS relative intensity ((■) $FeN_2C_4^+$ only; (○) $\Sigma FeN_2C_y^+$) as a function of the pyrolysis temperature.

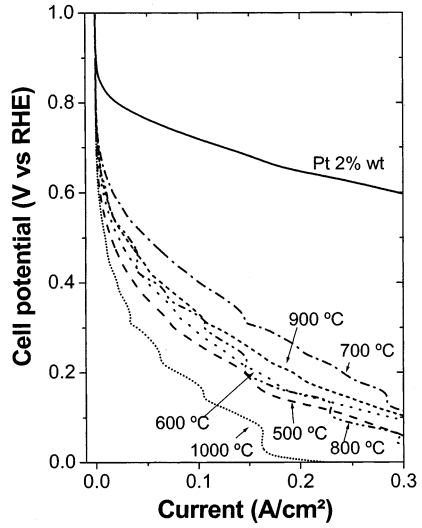

Figure 11. Effect of the pyrolysis temperature on the polarization curves for type II Fe(0.2) P catalysts. The polarization curve for Pt 2 wt % is given for comparison.

behavior of the catalysts and that the influence of FeN_4/C is again minor.

Catalysts Obtained from Cl-Fe^{III} TMPP; Samples of the Type IIFe(2.0)P. Figure 12 shows again a comparison of the RDE−ToF SIMS for type IIFe(2.0)P catalysts. The curve in Figure 12 A represents the current densities measured at 0.7 V vs RHE in GDE tests with type IIFe(2.0)P catalysts and their full polarization curves are given in Figure 13. The curve in Figure 12B represents the changes in relative abundance of the FeN_2/C site and is the same data as was shown in Figure 5C. The dark squares in Figure 12B represent the evolution with the pyrolysis temperature of $FeN_2C_4^+$, the main FeN_2/C site ion. It is obvious this time that no correlation exists between the two parts of Figure 12.

How to explain this lack of correlation, while strong correlations exist for the samples with Fe contents 10 times smaller? A plausible explanation is that, for II Fe(2.0)P catalysts, the ToF SIMS technique is not actually probing the active regions of these high Fe loaded catalysts. This reasoning make sense when the size of the porphyrin molecule and the Fe content for these IIFe(2.0)P catalysts are considered. Indeed, to obtain 2 wt % Fe, 0.458 g of Cl-FeTMPP was adsorbed onto 1.000 g of

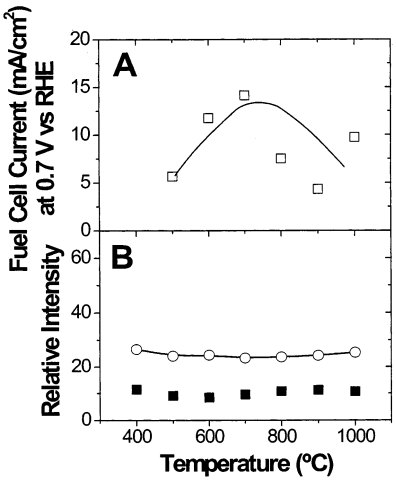

Figure 12. Type II Fe(2.0) P catalysts: Comparison between the catalytic activity (as fuel cell current) and the ToF SIMS relative intensity ((■) $FeN_2C_4^+$ only; (○) $\Sigma FeN_2C_y^+$) as a function of the pyrolysis temperature.

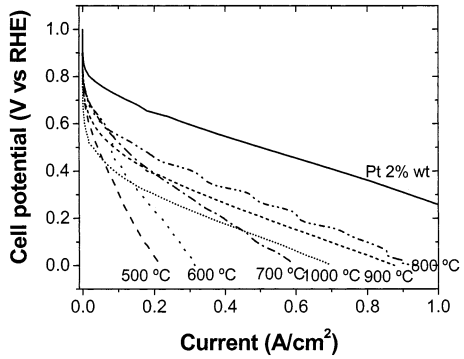

Figure 13. Effect of the pyrolysis temperature on the polarization curves for type II Fe(2.0) P catalysts. The polarization curve for Pt 2 wt % is given for comparison.

pyrolyzed PTCDA. It is known that phthalocyanines and porphyrins prefer to adsorb flat on carbon type supports.[50,51] The size of Cl-FeTMPP may be considered similar to that of tetracarboxyphenyl porphyrin, which has been shown to adsorb in a 4-fold symmetry on a freshly cleaved HOPG surface. The distance between two adjacent molecules has been estimated by STM experiments to be 1.90 ± 0.05 nm. Therefore, the surface covered by Cl-FeTMPP is a square of 1.9 × 1.9 nm^2. The specific area of PTCDA pyrolyzed at 900 °C in H_2/NH_3/Ar ambient is 236 ± 7 m^2/g (measured by BET). It is calculated that the amount of Cl-FeTMPP used to obtain an Fe content of 2 wt % is sufficient to cover 4.7 times the entire surface of the support, assuming it is covered to the same extent as its BET surface area. It is, therefore, a catalyst precursor with multiple layers of Fe porphyrins (∼5 layers) that is pyrolyzed. The resulting material is most likely a porous layer of decomposed porphyrin on top of the actual catalytic sites bound to the carbon support. ToF SIMS is a technique that probes only the first molecular layer of the material. In this case, therefore, it is not probing the actual surface of the carbon support, where catalytic sites are located. If this hypothesis is correct, the ions observed by ToF SIMS for type II Fe(2.0)P catalysts should be similar to those obtained for pyrolyzed Cl-FeTMPP alone. In Table 4 are given relative abundance of $FeN_xC_y^+$ ions for neat unpyrolyzed Cl-FeTMPP. By summing all ions of the N_2 family, one obtains 25% of relative intensity, a value very similar to that seen in Figure 12B (or Figure 5C) for $\Sigma FeN_2C_y^+$. To be completely exact, the comparison should be done on pyrolyzed Cl-FeTMPP, but this was not possible since this unsupported material sublimes before pyrolyzing.

TABLE 4: Relative Abundance in % of $FeN_xC_y^+$ Ions for Cl-FeTMPP

ions	relative intensity
$FeNC^+$	19.40
$FeNC_2^+$	10.28
$FeNC_3^+$	5.69
FeN_2C^+	4.21
$FeN_2C_2^+$	3.73
$FeN_2C_3^+$	3.69
$FeN_2C_4^+$	7.37
$FeN_2C_5^+$	3.26
$FeN_2C_6^+$	1.97
FeN_3C^+	2.75
$FeN_3C_2^+$	2.14
$FeN_3C_3^+$	4.13
$FeN_3C_4^+$	2.64
$FeN_3C_5^+$	2.35
$FeN_3C_6^+$	1.36
$FeN_3C_7^+$	1.76
$FeN_3C_8^+$	1.71
$FeN_3C_9^+$	2.64
FeN_4C^+	1.45
$FeN_4C_2^+$	2.00
$FeN_4C_3^+$	1.77
$FeN_4C_4^+$	0.66
$FeN_4C_5^+$	1.85
$FeN_4C_6^+$	1.55
$FeN_4C_7^+$	2.05
$FeN_4C_8^+$	2.74
$FeN_4C_9^+$	1.63
$FeN_4C_{10}^+$	1.18
$FeN_4C_{11}^+$	0.88
$FeN_4C_{12}^+$	1.15

To end this section, it should be mentioned that $FeN_2C_4^+$ is not an important ion in the fragmentation of Cl-FeTMPP$^+$. Indeed, according to Table 4, it represents only about 7% of all $FeN_xC_y^+$ ions listed in the table. It should also be mentioned that the ions listed in Tables I−IV do not include the whole ensemble of all possible $FeN_xC_y^+$ ions but a large fraction of them at sufficiently low mass that it is possible to assign them univocally to experimental peaks in the ToF SIMS spectra. There are, however, a few notable exceptions where high mass ions were univocally assigned to $FeN_xC_y^+$ ions. These are shown in Figure 14, where the ions $(FeTMPP \pm xH)^+$ are detected (Figure 14A) around 789 ± *x* amu in the spectrum of unsupported Cl-FeTMPP. This assignation is corroborated by the detection around 792 ± *x* amu of the $(CoTMPP \pm xH)^+$ ions in the spectrum of unsupported CoTMPP (Figure 14B). A change in the mass of the metal is responsible for the difference between these two high-mass ions. The largest detected $FeN_xC_y^+$ ion in the pyrolyzed Fe-based catalysts of this work has a mass of 452 amu (Figure 14C). This is corroborated by the detection of a peak at 455 amu (Figure 14D) in a catalyst of the type IICo(2.0)P, while the peak at 465 amu can obviously be assigned to an ion without metal content since it is present at the same amu in both Figures 14C and 14D.

Conclusions

Three types of catalysts based on Fe were produced for the electroreduction of O_2 in acidic medium. The goal was to compare their ToF SIMS and RDE (or GDE) behavior in order to find similar trends in the results that could lead to structural information on the catalytic sites. To obtain meaningful results, it is important to consider several points:

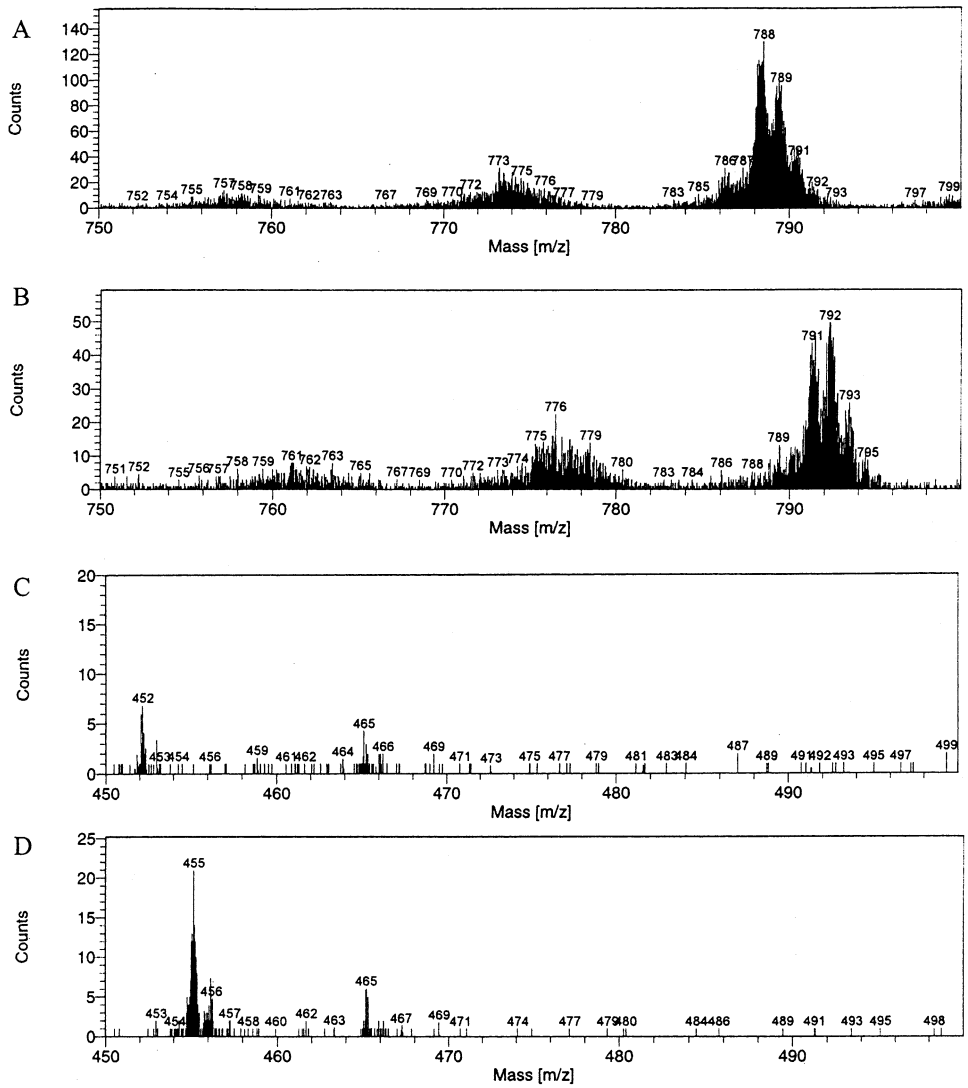

Figure 14. Selected amu ranges in ToF−SIMS spectra of: (A) Cl-FeTMPP; (B) CoTMPP; (C) II Fe(0.2)P type catalyst pyrolyzed at 900 °C; (D) II Co (2.0)P-type catalyst pyrolyzed at 900 °C.

(i) It is necessary to follow the variation of $FeN_xC_y^+$ ions in pyrolyzed catalysts by ToF SIMS since these three elements in these ions are necessary for catalytic activity.

(ii) Since $FeN_xC_y^+$ ions are characterized by a low relative abundance in the ToF SIMS spectra, it is important to use a low background carbon support like pyrolyzed PTCDA. If commercial carbon supports with a higher background are used, most of the $FeN_xC_y^+$ ions of relatively high mass will be lost in the background and erroneous conclusions may be reached.

(iii) It is also necessary to use low Fe loadings in order to avoid the detection of ions from structures containing Fe that have no catalytic activity.

When all these precautions are taken, the following conclusions are reached:

(i) Two different catalytic sites exist simultaneously at all pyrolysis temperatures (from 400 to 1000 °C) in catalysts made with an iron salt (Fe^{II} acetate) or an Fe porphyrin (Cl-Fe^{III} TMPP) as Fe precursor. Therefore, what were previously labeled as low- and high-temperature catalytic sites exist simultaneously and not independently at all pyrolysis temperatures.

(ii) One of the catalytic sites (labeled FeN_4/C) is characterized by ions of the $FeN_4C_y^+$ family as well as ions coming from two other families: $FeN_1C_y^+$ and $FeN_3C_y^+$. They have their origin from what was previously labeled the low-temperature catalytic site. The other catalytic site (labeled FeN_2/C) is characterized by the $FeN_2C_y^+$ family of ions, with $FeN_2C_4^+$ being the main ion in that family. These ions have their origin from what was previously labeled the high-temperature catalytic site, a proposed partial structure of which is illustrated in Figure 1.

(iii) The abundance of the FeN_2/C catalytic site goes through a maximum in the pyrolysis temperature range from 700 to 900 °C, depending upon the Fe precursor (800−900 °C for Fe acetate; 700−800 °C for Cl-FeTMPP). This maximum abundance of the FeN_2/C ion family corresponds to a minimum abundance of the FeN_4/C family For catalysts prepared from Fe acetate, FeN_2/C is the main catalytic site and may represent up to 80% of the two catalytic sites in these materials. Perhaps, surprisingly the FeN_4/C site is also found for the catalysts prepared with the acetate as precursor. When porphyrin is used as Fe precursor, an FeN_4/C catalytic site is expected since this structure is already present in the structure of the precursor. However, FeN_2/C is also found and its abundance may reach up to 50%.

(iv) One important finding is that FeN_2/C is more active than the FeN_4/C catalytic site, since the variation in the RDE (or GDE) ORR results for catalysts prepared at different pyrolysis temperatures was only reflected commensurably by the change of relative abundance of FeN_2/C ion family detected by ToF SIMS. The reason FeN_2/C is more active than FeN_4/C in

catalysts obtained by pyrolysis is not known. One possible explanation might be that the FeN_2/C catalytic site is in better electrical contact with the graphene plane (see Figure 1) than FeN_4/C, which is more difficult to integrate in the structure of the graphene plane or on its edge. However, this is only an hypothesis that should be demonstrated.

(v) Finally, it has been shown that the FeN_2/C and FeN_4/C catalytic sites obtained at high Fe porphyrin loadings (2.0 wt % Fe) are covered with a porous structure of pyrolyzed Cl-FeTMPP. This porous layer is the structure probed by ToF SIMS and it is for this reason that a correlation is not found between ToF SIMS and RDE (or GDE) results for the high Fe porphyrin loaded samples.

Acknowledgment. The authors thank C. Poleunis for his technical help with SIMS measurements. They also acknowledge NSERC and the "Québec/Wallonie-Bruxelles" cooperation for their financial support. J.P.D. thanks Mark Lefebvre from MPI for suggestions and comments.

References and Notes

(1) Gottesfeld, Sh.; Zawodzinski, T. A. *Adv. Electrochem. Sci. Eng.* **1997**, *5*, 195.
(2) Wiesener, K. *Electrochim. Acta* **1986**, *31*, 1073.
(3) Wiesener, K.; Ohms, D.; Neumann, V.; Franke, R. *Mater. Chem. Phys.* **1989**, *22*, 457.
(4) Tarasevich, M. R.; Zhutaeva, G. V.; Radyushkina, K. A. *Russ. J. Electrochem. (Trans. of Electrokhimiya*) **1995**, *31*, 1064.
(5) Tarasevich, M. R.; Radyuskina, K. A. *Mater. Chem. Phys.* **1989**, *22*, 477.
(6) Scherson, D.; Tanaka, A. A.; Gupta, S. L.; Tryk, D.; Fierro, C.; Holze, R.; Yeager, E. B.; Latimer, R. P. *Electrochim. Acta* **1986**, *31*, 1247.
(7) Tanaka, A.; Gupta, S. L.; Tryk, D.; Fierro, C.; Yeager E. B.; Scherson, D. A. In *Structural Effects in Electrocatalysis and Oxygen Electrochemistry*; Scherson, D., Tryk, D., Daroux, M., Xing, X., Eds.; The Electrochemical Society Inc., Pennington, NJ, 1992; *92-11*, p 555.
(8) Gojkovic, S. Lj.; Gupta, S.; Savinell, R. F. *J. Electrochem. Soc.* **1998**, *145*, 3493.
(9) Gojkovic, S. Lj.; Gupta, S.; Savinell, R. F. *J. Electroanal. Chem.* **1999**, *462*, 63.
(10) Gojkovic, S. Lj.; Gupta, S.; Savinell, R. F. *Electrochim. Acta* **1999**, *45*, 889.
(11) van Veen, J. A. R.; Colijn, H. A.; van Baar, J. F. *Electrochim. Acta* **1988**, *33*, 801.
(12) Sun, G. Q.; Wang, J. T.; Gupta, S.; Savinell, R. F. *J. Appl. Electrochem.* **2001**, *31*, 1025.
(13) Bouwkamp-Wijnoltz, A. L.; Visscher, W.; van Veen, J. A. R. *Electrochim. Acta* **1998**, *43*, 3141.
(14) Biloul, A.; Gouérec, P.; Savy, M.; Scarbeck, G.; Besse, S.; Riga, J. *J. Appl. Electrochem.* **1996**, *26*, 1139.
(15) Gouérec, P.; Biloul, A.; Contamin, O.; Scharbeck, G.; Savy, M.; Riga, J.; Weng, L. T.; Bertrand, P. *J. Electroanal. Chem.* **1997**, *422*, 61.
(16) Gouérec, P.; Savy, M.; Riga, J. *Electrochim. Acta* **1998**, *43*, 743.
(17) Gouérec, P.; Savy, M. *Electrochim. Acta* **1999**, *44*, 2653.
(18) Contamin, O.; Debiemme-Chouvy, C.; Savy, M.; Scarbeck, G. *Electrochim. Acta* **1999**, *45*, 721.
(19) Contamin, O.; Debiemme-Chouvy, C.; Savy, M.; Scarbeck, G. *J. New Mater. Electrochem. Systems* **2000**, *3*, 67.
(20) Ladouceur, M.; Lalande, G.; Guay, D.; Dodelet, J. P.; Dignard-Bailey, L.; Trudeau, M. L.; Schulz, R. *J. Electrochem. Soc.* **1993**, *140*, 1974.
(21) Lalande, G.; Côté, R.; Tamizhmani, G.; Guay, D.; Dodelet, J. P.; Dignard-Bailey, L.; Weng, L. T.; Bertrand, P. *Electrochim. Acta* **1995**, *40*, 2635.
(22) Faubert, G.; Côté, R.; Guay, D.; Dodelet, J. P.; Dénes, G.; Bertrand, P. *Electrochim. Acta* **1998**, *43*, 341.
(23) Sawaguchi, T.; Itabashi, T.; Matsue T.; Uchida, I. *J. Electroanal. Chem.* **1990**, *279*, 219.
(24) Widelöv, A. *Electrochim. Acta* **1993**, *38*, 2493.
(25) Claude, E.; Addou, T.; Latour, J. M.; Aldebert, P. *J. Appl. Electrochem.* **1998**, *28*, 57.
(26) Okada, T.; Gokita, M.; Yuasa, M.; Sekine, I. *J. Electrochem. Soc.* **1998**, *145*, 815.
(27) Okada, T.; Gotou, S.; Yoshida, M.; Yuasa, M.; Hirose, T.; Sekine, I. *J. Inorg. Organomet. Polym.* **1999**, *9*, 199.
(28) Okada, T.; Yoshida, M.; Hirose, T.; Kasuga, K.; Yu, T.; Yuasa, M.; Sekine, I. *Electrochim. Acta* **2000**, *45*, 4419.
(29) Jiang, R.; Chu, D. *J. Electrochem. Soc.* **2000**, *147*, 4605.
(30) van Wingerden, B.; van Veen, J. A. R.; Mensch, C. T. J. *J. Chem. Soc., Faraday Trans. 1* **1988**, *84*, 65.
(31) Lefèvre, M.; Dodelet, J. P.; Bertrand, P. *J. Phys. Chem. B* **2000**, *104*, 11238.
(32) Bae, I. T.; Tryk, D. A.; Scherson, D. A. *J. Phys. Chem. B* **1998**, *102*, 4114.
(33) Gupta, S.; Tryk, D.; Bae, I.; Aldred, W.; Yeager, E. *J. Appl. Electrochem.* **1989**, *19*, 19.
(34) Ohms, D.; Herzog, S.; Franke, R.; Neumann, V.; Wiesener, K.; Gamburcev, S.; Kaisheva, A.; Iliev, I. *J. Power Sources* **1992**, *38*, 327.
(35) Martin Alves, M. C.; Tourillon, G. *J. Phys. Chem.* **1996**, *100*, 7566.
(36) Lalande, G.; Côté, R.; Guay, D.; Dodelet, J. P.; Weng, L. T.; Bertrand, P. *Electrochim. Acta* **1997**, *42*, 1379.
(37) Fournier, J.; Lalande, G.; Côté, R.; Guay, D.; Dodelet, J. P. *J. Electrochem. Soc.* **1997**, *144*, 218.
(38) Côté, R.; Lalande, G.; Guay, D.; Dodelet, J. P.; Dénès, G. *J. Electrochem. Soc.* **1998**, *145*, 2411.
(39) Côté, R.; Lalande, G.; Faubert, G.; Guay, D.; Dodelet, J. P.; Dénès, G. *J. New Mater. Electrochem. Systems* **1998**, *1*, 7.
(40) Faubert, G.; Côté, R.; Guay, D.; Dodelet, J. P.; Dénès, G.; Poleunis, C.; Bertrand, P. *Electrochim. Acta* **1998**, *43*, 1969.
(41) Wang, H.; Côté, R.; Faubert, G.; Guay, D.; Dodelet, J. P. *J. Phys. Chem. B* **1999**, *103*, 2042.
(42) Bouwkamp-Wijnoltz, A. L.; Visscher, W.; van Veen, J. A. R.; Tang, S. C. *Electrochim. Acta* **1999**, *45*, 379.
(43) Wei, G.; Wainright, J. S.; Savinell, R. F. *J. New Mater. Electrochem. Systems* **2000**, *3*, 121.
(44) Faubert, G.; Côté, R.; Dodelet, J. P.; Lefèvre, M.; Bertrand, P. *Electrochim. Acta* **1999**, *44*, 2589.
(45) He, P.; Lefèvre, M.; Faubert, G.; Dodelet, J. P. *J. New Mater. Electrochem. Systems* **1999**, *2*, 243.
(46) Dignard-Bailey, L.; Trudeau, M.; Joly, A.; Schulz, R.; Lalande, G.; Guay, D.; Dodelet, J. P. *J. Mater. Res.* **1994**, *9*, 3202.
(47) Van den Brink, F.; Barendrecht, E.; Visscher, W. *Recl. Trav. Chim. Pays-Bas* **1980**, *99*, 253.
(48) Zagal, J. H. *Coord. Chem. Rev.* **1992**, *119*, 89.
(49) Sono, M.; Roach, M. P.; Coulter, E. D.; Dawson, J. H. *Chem Rev.* **1996**, *96*, 2887.
(50) Jiang, D.; Zhao, B.; Huang, H.; Xie, Y.; Pan, G.; Ran, G.; Min, E. *Appl. Catal. A: General* **2000**, *192*, 1.
(51) Lei, S. B.; Wang, C.; Yin, S. X.; Wang, H. N.; Xi, F.; Liu, H. W.; Xu, B.; Wan, L. J.; Bai, C. L. *J. Phys. Chem. B* **2001**, *105*, 10838.